Citation: Molecular Therapy — Methods & Clinical Development (2016) **5,** 16070; doi:10.1038/mtm.2016.70
Official journal of the American Society of Gene & Cell Therapy

www.nature.com/mtm

ARTICLE

Assessment of murine colorectal cancer by micro-ultrasound using three dimensional reconstruction and non-linear contrast imaging

Jessica L Freeling[1] and Khosrow Rezvani[1]

The relatively low success rates of current colorectal cancer (CRC) therapies have led investigators to search for more specific treatments. Vertebrate models of colorectal cancer are essential tools for the verification of new therapeutic avenues such as gene therapy. The evaluation of colorectal cancer in mouse models has been limited due to the lack of an accurate quantitative and longitudinal noninvasive method. This work introduces a method of three-dimensional micro-ultrasound reconstruction and microbubble administration for the comprehensive and longitudinal evaluation of CRC progression. This approach enabled quantification of both tumor volume and relative vascularity using a well-established inducible murine model of colon carcinogenesis. This inducible model recapitulated the adenocarcinoma sequence that occurs in human CRC allowing systematic *in situ* evaluation of the ultrasound technique. The administration of intravenous microbubbles facilitated enhancement of colon vascular contrast and quantification of relative vascularity of the mid and distal colon of the mouse in three dimensions. In addition, two-dimensional imaging in the sagittal orientation of the colon using Non-Linear Contrast Mode enabled calculation of relative blood volume and perfusion as the microbubbles entered the colon microvasculature. Quantitative results provided by the outlined protocol represent a noninvasive tool that can more accurately define CRC development and progression. This ultrasound technique will allow the practical and economical longitudinal study of murine CRC in both basic and preclinical studies.

Molecular Therapy — Methods & Clinical Development (2016) **5**, 16070; doi:10.1038/mtm.2016.70; published online 30 November 2016

INTRODUCTION

Despite advances in early detection and treatment, over 100,000 men and women are diagnosed with colorectal cancer (CRC) and more than 50,000 die from the disease each year in the United States.[1] CRC is a major cause of cancer deaths worldwide[2] and it has been predicted that the number of patients with CRC will reach above 2.2 million new cases (60% increase) with 1.1 million deaths by 2030.[3] While advances in screening strategies and treatment regimens have improved overall survival rates, 50% of colorectal carcinoma patients develop recurrent disease, with an overall 5-year survival rate of 6–12%.[4] Thus, a major challenge in the management of CRC is the development of novel targets for the therapy of CRC which can improve the current chemotherapeutic regimen.

The published literature over the last decade has verified animal models as reliable preclinical models to test cancer therapeutic strategies. Three primary types of *in vivo* CRC models are employed in mice: xenograft, orthotopic, and inducible models. While xenograft models have been used readily, these models have limited utility due to their inability to fully recapitulate disease metabolism and macroenvironment complexity.[5] Due to the limitations of xenograft studies, the *in vivo* murine models of CRC have been optimized for a variety of mechanistic and drug-development studies in the last decade.[6–8] Among the *in vivo* mouse models, the inducible model type is less invasive than orthotopic models[7] and able to closely recapitulate the macroenvironment of CRC, including growth and metabolism.[8,9] In addition to inducible CRC models, genetic manipulation or the use of genetically susceptible mouse models have become ideal tools for CRC research. These models are particularly valuable when the functions of genes and their protein networks in CRC are the focus of study.[10] A well-established murine model for the chemical induction of colon carcinogenesis employs azoxymethane (AOM) and dextran sodium sulphate (DSS) compounds.[6,11–13] The generation, stage-dependent progression, localization, and molecular profile of AOM-induced tumors closely mimics human CRC.[6] However, with the advent of a fully inducible, *in vivo* model of CRC, comes the difficulty in establishing a reliable longitudinal and quantitative method for monitoring the progression of the disease. This is particularly challenging in a small-sized animal model.

Minimally invasive imaging of orthotopic or inducible types of CRC in mice can potentially be facilitated by multiple methods including; optical colonoscopy (OC),[14–16] magnetic resonance imaging,[17,18]

[1]Division of Basic Biomedical Sciences, Sanford School of Medicine, The University of South Dakota, Vermillion, South Dakota, USA; Correspondence: JL Freeling (jessica.freeling@usd.edu) or K Rezvani (khosrow.rezvani@usd.edu)
Received 17 July 2016; accepted 26 September 2016

x-ray computed tomography (CT),[19] optical coherence tomography (OCT),[20] endoluminal ultrasonic biomicroscopy,[21] and 2D Brightness mode (B-mode) micro-ultrasound.[22] Despite improvements and optimizations, the broad employment of these methods has been limited. Therefore, methods for the evaluation of CRC tumor burden in the mouse commonly include endpoint quantification or the use of invasive techniques which do not enable adequate longitudinal evaluation due to necessity of termination of mice at multiple time-points.[23] Commonly employed techniques are scale-based scoring systems to estimate tumors and/or measure two dimensional tumor areas from photographs or histology slides collected at necropsy.[8,15,23,24] While other means of evaluating changes in colon morphology, such as measurement of colon length and weight are valid and remain integral to CRC evaluation, these cannot be performed *in vivo* and longitudinally over the course of cancer progression. Traditional two dimensional microultrasonography (2D ultrasound) employed in mouse models of CRC is limited to a single-plane view of individual tumors and provides no information about total tumor burden or quantification of vascularity.[22] Indeed, both 2D ultrasound and standard photographic images ignore the complexity and dynamics of developing tumors and therefore by definition, can only provide tumor area and not volume.

In this study, we present a straightforward technique for three-dimensional (3D) reconstruction of the entire mid and distal colon of the mouse with and without tumors using 3D Mode on the Vevo 2100 Micro-Ultrasound System. 3D Mode ultrasound captured hundreds of individual image-slices (in essence "Z-stacks" the slices together), enabling user-defined reconstruction of the mid and distal colon with associated tumors. Our optimized method produced quantitative volume data facilitating determination of treatment paradigms in live animals. Data collected during tumor progression in live animals confirmed the advantage of this method over traditional endpoint-only measures. Additionally, through the use of nontargeted microbubble contrast agents (see Methods section) and 2D Non-Linear Contrast Mode (2D NLC Mode) with associated VevoCQ software, we determined the relative vascularity of colon tissues in the presence and absence of CRC. These data enabled quantification of relative vascularity via calculations using percent agent (PA, obtained from 3D reconstructions), and relative blood volume and perfusion (obtained from 2D sagittal images), providing multiple advantages over previous CRC evaluation techniques.[7,21,22] This approach included the opportunity to acquire tumor load data at multiple stages of colon cancer progression. This straightforward, reproducible, and noninvasive method provides an *in vivo* and real-time assessment of tumor burden in any type of murine CRC model. Quantitative measurement of changes in colon morphology (volume, thickness, and length) and tumor parameters (number, volume, and location) and their vascularization over the course of disease, with and without treatments, can provide valuable data for clinical pharmacology of anticancer drugs.

RESULTS

Definitions of gross colon anatomy

Figure 1 illustrates the gross anatomy nomenclature of the mouse lower gastrointestinal tract.[25] The large intestine of the mouse can be roughly divided into three segments; the proximal colon originating from the ileocecal junction, the midcolon, and the distal colon.[26] Each segment represents approximately one-third of the total colon length. The proposed imaging technique enabled evaluation of the entire mid and distal colon, beginning approximately at the *flexure* in the colon and ending at the anus as depicted in Figure 1. The

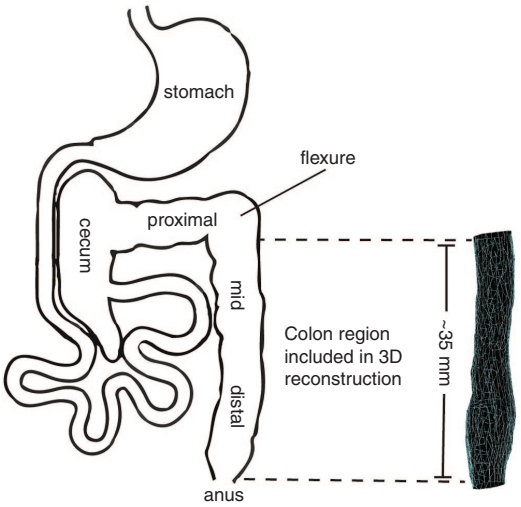

Figure 1 Definition of mouse colon gross anatomy. The murine colon is equally divided into three segments consisting of the proximal, mid, and distal colon. During i*n vivo* ultrasound imaging, a *flexure* between the mid and proximal colon sections is clearly visible, providing a landmark for image acquisition and analysis using the proposed technique. The mid and distal colon sections together are ~ 35 mm in length in a 3–4 months old, 30 g mouse.

mouse, unlike the human, lacks a rectum and exhibits a single *flexure*. The *flexure* is clearly identifiable during ultrasound imaging and serves as a ubiquitous landmark for uniformity of image acquisition and analysis. The mid and distal colon of the mouse is located in the medial plane of the abdomen and is unbending from the anus to the single *flexure* as diagrammed. Anatomical planes are defined using standard definitions in Figure 2a with the sagittal plane representing the longitudinal axis and the transverse plane representing the horizontal axis of the animal.

3D micro-ultrasound reconstruction and visualization of the mid and distal colon

Using the Vevo 2100 micro-ultrasound system, noninvasive images were collected through the abdomen in the lightly-anesthetized mouse. The ability to collect high-quality ultrasound images of the diminutive mouse colon was largely dependent on two simple techniques. First, standard ultrasound gel (US gel) was administered retrograde within the colon via the anus. This necessary step enabled distension of the colon lumen providing enhanced contrast and visualization of the colon. The US gel within the colon enabled clear identification of tumor structures and their attachment to the luminal surfaces of the mid and distal colon. Second, subcutaneous delivery of a short-acting form of atropine allowed the halting of intestinal peristaltic waves enabling retention of the intracolon gel, facilitating the 3D-mode reconstruction of clear images (see Methods). The basic method of 3D-mode colon reconstruction in the mouse in depicted in Figure 2. The MS550S ultrasound transducer was attached to a 3D-Motor which controls the transducer as a series of several hundred individual high-resolution 2D B-mode ultrasound images were acquired. These images included the mid and distal colon and encompassed a maximal scan distance of ~35 mm. The individual 2D image slices were acquired along the transverse plane (Figure 2a) and assembled ("Z-stacked") to create an integrated 3D-image (Figure 2b, Supplementary Video S1). The user then defined the boundaries

of the colon walls and associated tumors from which volume data was acquired. The result is a 3D graphic reconstruction of the entire mid and distal colon (Figure 2c, Supplementary Video S2). Multiple options for graphical representation of reconstruction data renderings are available in the VevoLAB software (Figure 3). From these reconstructions, individual tumor volumes can be extracted if desired. The user-friendly software allows accurate calculation of individual tumor volume and total tumor volume load in an

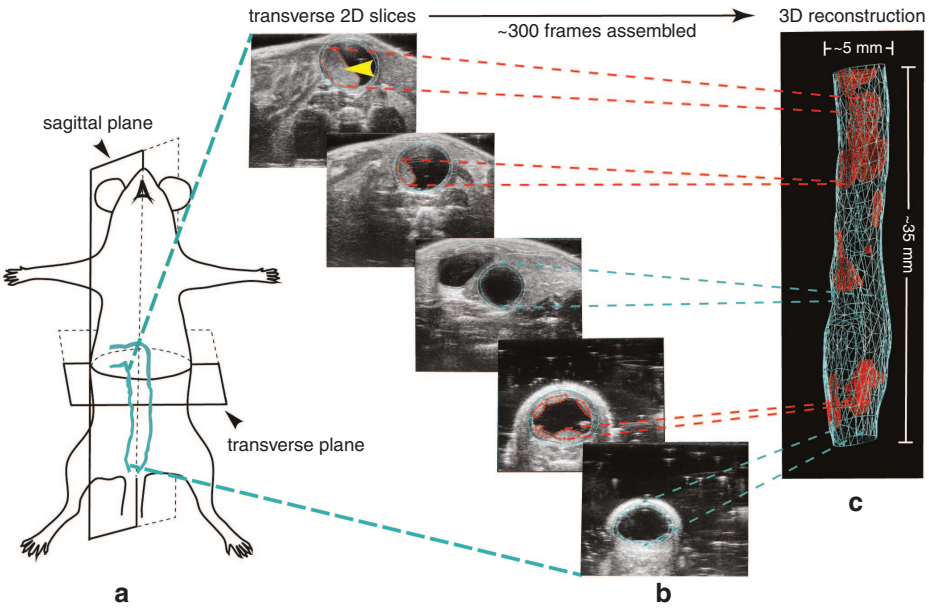

Figure 2 Ultrasound colon image acquisition in the mouse model and 3D reconstruction. (**a**) The sagittal and transverse planes are defined. More than 300 individual transverse image slices are obtained encompassing the mid/distal colon and anus of the mouse using a micro-ultrasound system equipped with 3D Motor to control the transducer. (**b**) Depicted is an example of just five of the 344 B-mode image slices obtained. Note the clarity of the tumor denoted with the yellow arrow. (**c**) Using user-friendly VevoLAB software, the inner and outer colon walls, as well as each individual tumor are defined. Image slices are then assembled together for a 3D reconstruction of the colon and associated tumors. Blue and red lines are graphical representations of colon walls and tumors, respectively.

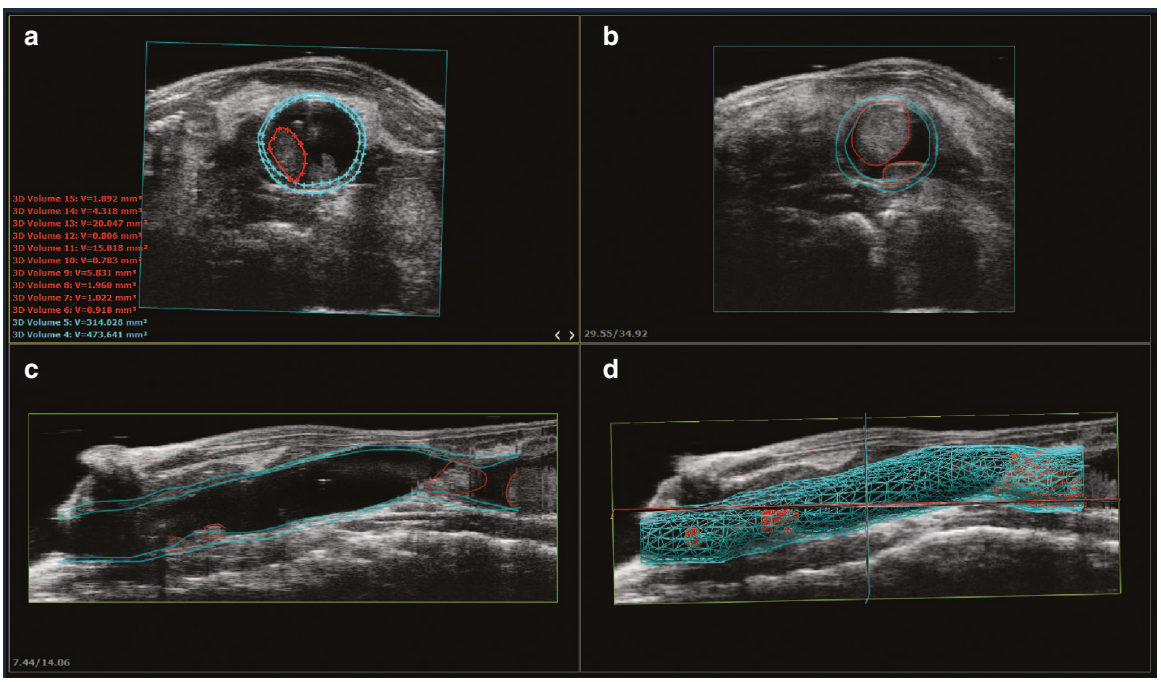

Figure 3 Display options of 3D reconstructed data. The VevoLAB software provides multiple viewing options of 3D reconstructed data renderings. (**a**) An example transverse colon slice with user-defined regions of interest (ROI) of colon walls (light blue) and tumor (red). Individual ROI volumes are available as export from the software enabling the user to quantify individual tumors or perform summation for total tumor load or colon wall load. (**b**) An example extrapolated transverse layer ROI applied by the software. (**c**) An example sagittal layer ROI produced by assemblage of the individual transverse layer ROIs. The anal end is shown at the left of the screen window. (**d**) A final 3D reconstruction depicting all applied ROIs with the ultrasound data overlay visible around the reconstructed colon.

exportable format. In addition, the software allowed measurement of the thickening of the mid and distal colon wall in the form of total wall volume. Changes in the thickness of the colon and rectal walls can be caused by neoplastic, inflammatory, infectious, or even ischemic conditions.[27] Detecting focal, segmental, or diffuse wall thickening offers unique capabilities and provides valuable insight into cancer phenotypes and tumor responses to drug treatment. The ability to evaluate colon wall volume therefore provides additional benefit to the study of ischemic, infectious, and inflammatory diseases in the lower digestive system of the mouse.

3D assessment of the scope of tumor progression in the colon—A case series analysis

Based on the results presented in Figure 2, we hypothesized that the high-quality assessment of colon structures using these 3D reconstruction techniques would further provide a critical and accurate longitudinal assessment of CRC in mouse models. To address this hypothesis, AOM/DSS, a well-established method for the induction of colon carcinogenesis in mice was used.[8] The AOM/DSS treated mice predominantly generated tumors in the distal colon and anus, recapitulating the adenocarcinoma sequence that occurs in human CRC.[6] Normal wildtype C57BL/6 mice exposed to AOM/DSS to induce CRC were treated either with vehicle (WT+VEH) or with an anticancer compound under investigation in our group (WT+TX). The aforementioned 3D-mode ultrasound reconstructions were recorded at multiple time points throughout the experiment to monitor the progression of CRC. Ultrasounds were conducted at pretreatment, post-treatment, and terminal time-points to evaluate longitudinal progression (Figure 4e). Each time-point was compared with and without treatment. Figure 4a–d illustrates 3D-mode colon reconstructions of a representative animal from each group alongside matched traditional photographic images of tumors in the mid and distal colon after sacrifice of animals. Importantly, the depicted 3D reconstructions provide total tumor volume (mm^3) (Figure 4a–c) while photographic images only offer 2D tumor surface area (mm^2). Our optimized technique demonstrates the capability of this approach to accurately trace tumor growth and measure the responses of tumors to treatment in live animals. This approach can become a standard, reliable, and noninvasive tool that complements current strategies used to study solid tumors in mouse models of colon cancer.

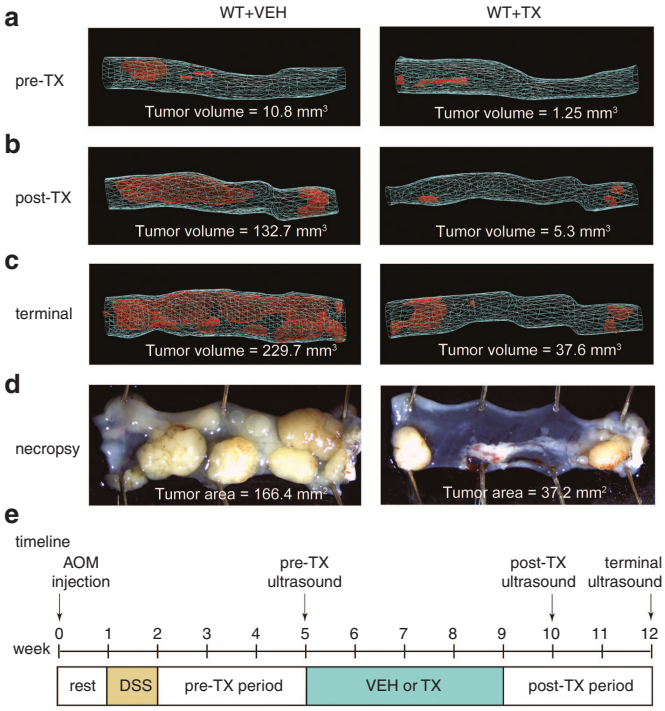

Figure 4 3D reconstructions of colons provides a quantitative measurement of tumor dynamics with and without treatments. All time-points represent WT animals challenged with azoxymethane (AOM)/dextran sodium sulphate (DSS) to induce colorectal cancer 5 weeks prior to the beginning of treatment with Treatment X (TX) or Vehicle (VEH). The anal-end is depicted at right in each image. (**a**) Prior to beginning TX or VEH, colons exhibited a small tumor volume load (VEH = 10.8 mm^3, TX = 1.25 mm^3). (**b**) Treatment for 5 weeks, resulted in a reduced tumor volume load compared with the VEH treated mouse (VEH = 132.7 mm^3, TX = 5.3 mm^3). (**c**) At termination, 7 weeks after beginning treatment, the animal given TX showed a dramatic difference in total volume load (VEH = 229.7 mm^3, TX = 37.6 mm^3). (**d**) Segment-matched photographic images of the mid and distal colon at necropsy with associated tumor areas (VEH = 166.4 mm^2, TX = 37.2 mm^2). (**e**) Diagram represents a timeline of the treatment paradigm.

Measuring vascular perfusion of colons containing disparate tumor loads with microbubble contrast-enhanced microultrasonography

Literature indicates the vascular perfusion of tumors can vary significantly due to tumor size, alteration of tumor-derived angiogenesis during tumor growth, or with exposure to postchemotherapy treatment.[28,29] We hypothesized that systemic administration of nontargeted microbubbles would enable differentiation and quantification of relative blood vascularity in colons carrying different sizes of tumors. Optimization of this approach can provide accurate criteria for the discrimination of advanced or nonresponsive tumors containing higher levels of perfusion, from abated or treated tumors having lower perfusion. To examine this hypothesis, at the terminal time-point, additional ultrasound data was collected through the use of intravenous administration of nontargeted microbubbles. It is noteworthy that the microbubble technique is not limited to endpoint collection and can be performed at any point during the execution of experiments using lateral tail vein injections (see Discussion). Two separate acquisition procedures, using a single microbubble injection, were performed. First, 2D NLC Mode was utilized to evaluate the relative blood perfusion and volume as the microbubbles infiltrated the distal colon (Figure 5). Second, 3D nonlinear contrast percent agent (3D NLC PA), enabled calculation of relative vascularity in three dimensions as the microbubbles circulated in the mid and distal colon vasculature.

2D NLC Mode was performed with the MS250 transducer, as NLC imaging requires a lower frequency to operate, making the higher resolution MS550S transducer unsuitable for NLC imaging. 2D NLC Mode with associated VevoCQ Software, was therefore used to analyze the slope and plateau of the infiltration of the injected microbubbles as they entered the vascular network encompassing the colon. Due to the nature of microbubbles which infiltrate very quickly, much more rapidly than the acquisition of 3D image slices can be obtained, the images were only acquired in 2D, rather than in 3D. In addition, by turning the transducer from the transverse to the sagittal orientation over the length of the colon, a larger surface area of the colon could be observed and quantified. A video of the wash-in of the microbubbles was recorded and analyzed using VevoCQ software (Supplementary Video S3). Figure 5 illustrates the sagittal images of the distal colon prior to (Figure 5a) and after (Figure 5b) the intravenous injection of microbubbles using three examples with disparate tumor populations. The maximum intensity persistence (MIP) of each image is provided (Figure 5c)

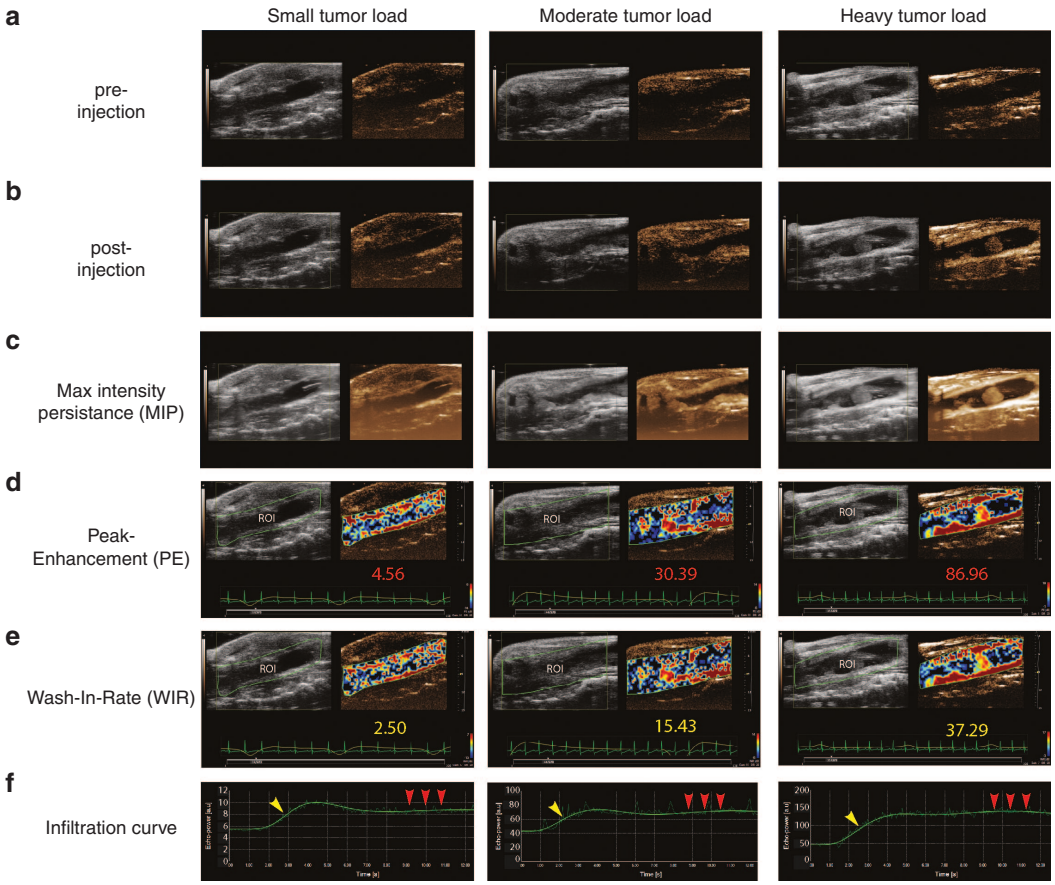

Figure 5 2D Non-Linear Contrast Mode enables calculation of relative blood volume and perfusion of the distal colon using intravenous nontargeted microbubbles. (**a**) 2D B-mode micro-ultrasound image of sagittal view prior to injection of microbubbles in three distal colons with disparate tumor loads (small, moderate, and heavy). (**b**) 2D B-mode micro-ultrasound image of sagittal view of the distal colon after the injection of microbubbles. (**c**) Maximum intensity persistence (MIP) providing enhanced visualization of microbubble perfusion indicating areas of vascularization. (**d**) The Peak Enhancement (plateau of the microbubble infiltration curve) provides quantification of relative blood volume. Quantified values for each of the colons is shown in red (small = 4.56 a.u., moderate = 30.39 a.u., heavy = 86.96 a.u.). (**e**) The wash-in-rate (slope of the microbubble infiltration curve) provides quantification of the relative blood perfusion. Quantified values for each of the colons is shown in yellow (small = 2.50 a.u., moderate = 15.43 a.u., heavy = 37.29 a.u.). (**f**) Microbubble infiltration curves for each of the colons. Note that the arbitrary unit (a.u.) y-axis scales are dramatically different between the three disparate tumor loads. The curve signatures are homologous indicating consistent kinetics between animals.

to enable enhanced visualization. Using MIP allowed us to accumulate and overlay the pixels from each frame which are alight as the microbubbles oscillate postinjection (also see Supplementary Video S4). For analysis, the user defined the region of interest (ROI), as depicted as the green border encompassing the B-mode image of the colon in each Figure 5d,e. The software then calculated parameters reflective of the relative blood volume (peak enhancement, Figure 5d) and relative blood perfusion (wash-in rate, Figure 5e) depicted as a parametric color image overlaid on the NLC contrast image in each Figure 5d,e. Associated quantifications of each of these parameters are included underneath the images. The slope (Figure 5f, yellow arrow) of the infiltration of the microbubbles as they enter the colon vasculature was reflective of the wash-in-rate and once the bubbles reached a stable plateau (Figure 5f, red arrows) in circulation this determined the PE. Note that the arbitrary unit (a.u.) y-axis scales provided by the VevoCQ software are dramatically different between the three disparate tumor load image examples. Reassuringly, the curve signatures were very similar suggesting consistent microbubble kinetics between animals.

While the NLC data obtained in Figure 5 is valuable as it can provide relative blood perfusion and volumes of the distal colon, this data is limited to a 2D image as the bubbles infiltrate the vessels of the colon in the sagittal plane. Because VevoCQ software cannot perform analysis in 3D, the 3D NLC PA technique was also performed. 3D NLC PA enables the determination of relative vascularity of the colon combining the capability of 3D reconstruction with that of NLC Mode. Using the same method as outlined for the 3D scan of the colon in Figure 2, the MS250 transducer oriented in the transverse plane is used to collect a 3D prescan but with NLC Mode and respiratory gating activated (see Methods). The transducer is then turned sagittal to enable the recording of the 2D NLC slope and plateau as previously outlined in Figure 5. This latter step was conducted with the respiratory gating turned off to avoid missing frames as the microbubbles infiltrated. Once the microbubbles were in circulation for several minutes, the transducer was returned to the transverse orientation, respiratory gating reactivated, and a subsequent 3D NLC PA postscan recorded. The absence and then subsequent presence of the microbubbles while injecting, enabled the software to perform a subtraction of the pre and postscans, thereby enabling quantification of the PA, representing the relative vascularity of the mid and distal colon in 3D. The 3D NLC PA values for the three example colons with disparate tumor loads (small, moderate, and heavy) depicted in Figure 5 were 6.3, 18.9, and 15.9% respectively. The increased level of relative vascularity from 6.3% in

the colon with the small tumor load to 18.9% in the colon with moderate tumor load matches literature reports of hyper vascularization of tumors.[30] The reduction in relative vascularity to 15.9% in the colon exhibiting a heavy tumor load may in fact reflect a reduction in relative vascularity due to the advanced state of tumor deterioration. Indeed, it is feasible that a reduction of microbubble infiltration in a colon with heavy loads of large tumors can be due to vessel malfunction.[31]

DISCUSSION

High-resolution micro-ultrasound systems are commonly available and employed for preclinical imaging.[32] These systems are more widely available to researchers than any other noninvasive *in vivo* imaging modality, with at least one VisualSonics Vevo micro-ultrasound unit at over 90 of the top 100 NIH-funded institutions (Stephen Buttars MS, Personal Communication). Additionally, transabdominal 3D ultrasound techniques have been employed in mice for many other types of cancer such as liver metastasis and prostate cancer.[33] While the 3D micro-ultrasound reconstruction of xenograft tumors in mice has become mainstream, a simple and reproducible method for the noninvasive 3D ultrasound of *in vivo* colon cancer is absent from the literature. In addition, a recent investigation of the literature indicated that the majority of studies enlisting mouse models of CRC failed to adequately evaluate the outcomes of tumor development and progression beyond endpoint collections and microscopic evaluations.[8,24]

We optimized an ultrasound technique that can accurately monitor CRC tumor growth in live animals very safely. This technique is not only applicable to genetically and chemically induced CRC models, but also to CRC orthotopic models such as surgical transplantation models, enema models, microinjection models, and transanal low dose electrocoagulation models.[7] Additionally, given the clarity of the colon wall images obtained, this technique may prove useful in mouse models of colitis and inflammatory bowel disease.[34,35]

The ability to obtain high-quality and high-resolution ultrasound images of the mouse colon can be accomplished by these important means: (i) Fast animals overnight to eliminate the majority of feces from the colon, (ii) Administer short-acting atropine to inhibit intestinal peristalsis, (iii) Deliver US gel within the colon to enhance contrast, (iv) Use a 3D-Motor to acquire multiple image slices to enable 3D reconstruction of the entire mid and distal colon, and (v) Employ the injection of microbubbles to facilitate enhanced contrast and quantification of relative colon vascularity, blood perfusion, and blood volume.

While our study only employed microbubble data collection at endpoint, microbubbles can indeed be utilized longitudinally as they pose no risk to the health of the animal with repeated administration, particularly via tail injection by an experienced person. However, several factors limited our ability and choice to perform repeated microbubble administrations. First, in our hands, mice exhibiting CRC using the inducible AOM/DSS model are quite small; the mice may be somewhat dehydrated, particularly immediately after the induction phase (pretreatment time-point); and the mice used in our model, C57BL/6, have black tails, all contributing to increased difficulty of tail vein injection at multiple time-points. Second, the cost of microbubbles, while greatly decreasing with increasing availability, was limiting at the time of our study. We therefore, chose to administer a microbubble bolus via a surgically-placed jugular catheter to ensure their infusion, and thus administration occurred at endpoint only. It should also be highlighted that we delivered the microbubbles using a bolus injection without the use of a syringe pump. We delivered a small bubble volume with a short catheter and the peak enhancement and wash-in-rate data reflected consistent kinetic signatures. However, it is feasible that the rate of injection of the bubbles by-hand could be somewhat variable. Variability in the rate of injection among animals could feasibly impact microbubble kinetics. Therefore, the use of a syringe pump for microbubble delivery is strongly recommended. Despite these limitations, our microbubble technique accurately differentiated the perfusion of colon tissues carrying different sizes of tumors, generating high-quality quantitative data.

In our hands, the utilized microbubbles remained strongly in circulation without any visually discernable decreases in bubble concentrations for ~15 minutes. This is an important advantage which makes the microbubbles safe for repeated administration. Also important to note is that the utilized microbubbles (SIMB3-4, Advanced Microbubble Laboratories LLC) are formulated using a PEG-lipid, known to be more stable than PEG-stearate (Feshitan J, Personal Communication). However, there may be concern that the relatively rapid degradation of the microbubbles could impact data outcomes if images are acquired at inconsistent postinjection time-points between animals. Postinjection 2D NLC imaging is accomplished immediately so could not be impacted by microbubble degradation. However, it is feasible that 3D NLC image data could be impacted by microbubble degradation if length of acquisition time is excessive. The half-life of microbubbles is dependent on concentration, size, and the relative vascularity of the organ being imaged.[36,37] Additionally, microbubbles degrade in a non-linear fashion making prediction of half-life difficult.[38] As evidenced by the provided timeline, we were able to acquire all of the necessary 2D and 3D NLC data in under 4 minutes. We highlight the importance of a consistent timeline in the acquisition of images. In our study, if the quick acquisition of the postscan was delayed, we waited for the bubbles to completely disappear and repeated the entire microbubble sequence.

Although we chose to utilize nontargeted microbubbles for our study, the use of targeted microbubbles can further enhance tumor characterization. Targeted microbubbles are available commercially in prebound forms or they can be conjugated with selected markers to target vascular markers of disease. The vascular endothelial growth factor (VEGF)-conjugated microbubble is an example which is selective for angiogenic endothelium in the tumor vasculature. VEGF-microbubbles can therefore provide a means to specifically quantify tumor-associated vascularity rather than vascularity of the entire colon and associated tumors.[39]

Other reports of standard 2D B-mode ultrasonography of colon tumors have inferred that the tumor area needed to be 3.0 mm^2 in size to identify.[22] Extrapolating this area to estimate the volume, assuming a spheroid tumor, translates to a minimal tumor volume of ~20 mm^3. However, in our study, the Vevo 2100 system with MS550S transducer easily enabled measurement of tumors as small as 0.5 mm^3. It is noteworthy that in some animals we were able to detect tumors as small as 0.1 mm^3. Additionally, previous publications of 2D ultrasound colon imaging techniques indicated difficulty in the differentiation of feces from tumors. However, as described in Figure 6a,b, fecal pellets exhibit a distinct distal shadow effect that does not occur with tumors. Moreover, Color Doppler Mode may be used to evaluate the object in question for the presence of blood flow to aid in confirmation (Figure 6b). However, we did encounter late-stage tumors, particularly in the distal colon, which exhibited limited blood flow using Color Doppler. It has been reported that the epithelial microvascular blood increases during neoplastic transfor-

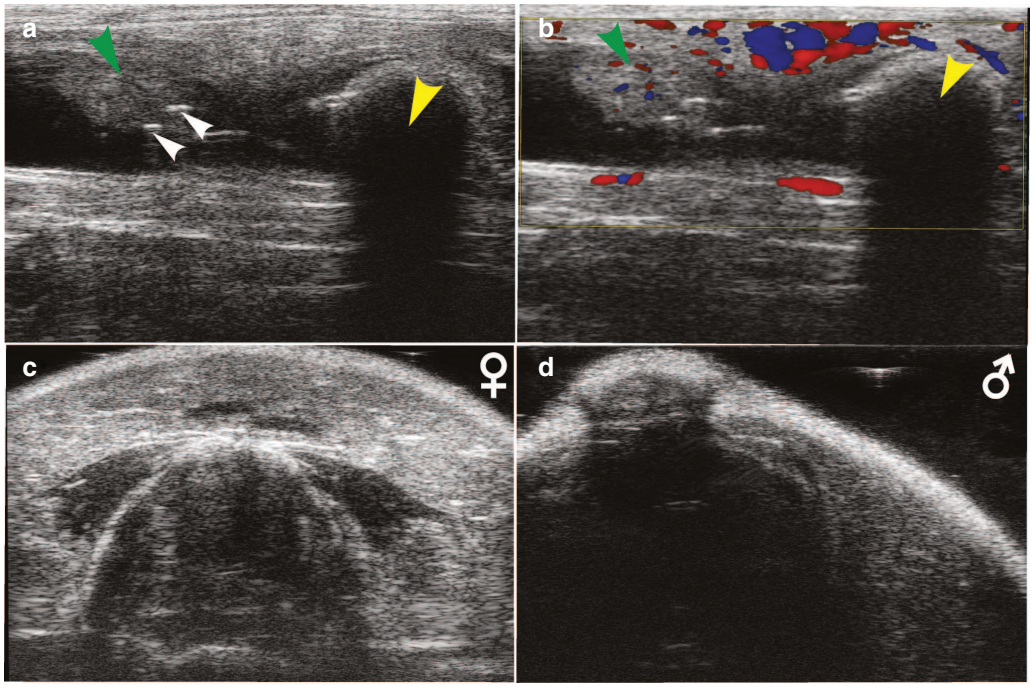

Figure 6 Identification of common ultrasound artifacts and obstructions. (**a**) 2D transverse ultrasound image of the mid colon depicting a tumor (green arrow), feces (yellow arrow), and bubbles in the ultrasound gel (white arrows). (**b**) Color-Doppler overlay showing presence of blood flow in the tumor (green arrow) but absence of blood flow in the feces (yellow arrow). Also note the appearance of a shadow effect below the feces that does not appear below the tumor. (**c**) Example transverse ultrasound image frame of female mouse while 3D Motor passes over the area of the vagina and pelvic bridge. (**d**) Example transverse image frame of male mouse while 3D Motor passes over the area of the penis/sheath and pelvic bridge.

mation as an early biological event in colorectal carcinogenesis.[30,40] Therefore, our optimized microbubble technique also has potential applicability for the visualization of colon perfusion during the premalignant stage in diverse CRC mouse models. Visualization of tumor vascularity enhanced understanding of tumor morphology and verification of tumor attachment to the intestinal wall.

Others have presented a method for 2D B-mode ultrasound in CRC.[22] The use of Color Doppler Mode imaging was suggested to visualize the blood flow to the colon and associated tumors. While this method provided acceptable visualization of tumors, the proposed method had two important limitations. First, the Vevo 2100 system and associated software does not offer the ability to quantify the collective blood flow obtained from Color Doppler Mode, and the associated Pulse Wave Mode can only quantify individual vessel flow. Second, their method only allowed the visualization of tumors in 2D. Therefore, our proposed technique using microbubbles and NLC Mode provides a distinct advantage, not only because of the ability to quantify the relative colon/tumor vascularity, but also this is accomplished in 3D.

The 3D ultrasound technique presented in this study has several distinct advantages over OC. While both techniques can evaluate changes in tumor size in serial observations, the 3D ultrasound shows more accuracy and precision in the measurement of tumors over OC. The primary reason is that OC provides only 2D estimates of tumor size, while the 3D ultrasound technique produces 3D tumor volumes.[14–16] As highlighted above, an accurate quantification of volume rather than width or area is essential to the evaluation of new anticancer compounds in CRC mouse models. In addition, Adachi *et al.* report that in the performance of 66 colonoscopies 120 tumors were found, but 107 tumors were missed, with the majority of missed tumors <3 mm in diameter. As previously explained, the resolution of the 3D ultrasound technique makes tumors of this size easily detectable. Finally, mortality rates are reported to be as high as 2.9% for OC, much higher than our 3D ultrasound technique, due to an increase in frequency of gut perforation.[16]

An additional advantage of our technique is that micro-ultrasound is already widely used for the preclinical evaluation of cardiac function in mice. Echocardiograms and associated cardiac function data are proving instrumental to preclinical research in the determination of whether chemotherapies are eliciting a cardiotoxic effect.[41,42] In fact, the mice in our study underwent echocardiograms just prior to colon imaging. It is important to note that the echocardiogram data should be collected prior to atropine administration to prevent blockade of the parasympathetic muscarinic receptor function of the heart, which could alter chronotropy and thus affect cardiac output. It is acknowledged that a change in cardiac output could therefore affect the peripheral vasculature blood flow and thus alteration of data acquired using microbubbles. However, it is suggested that the impact of atropine on the colon vasculature is minimal for several reasons. First, animals in our study exhibited an increase in heart rate of ~20 beats per minute from the time of echocardiogram data acquisition (pre-atropine administration) to delivery of microbubbles (post-atropine administration), indicating minimal cardiac parasympathetic blockade and therefore minimal impact on cardiac output (Supplementary Figure S5). Second, the utilized form of short-acting atropine resulted in a consistent increase in heart rate among experimental animals, making comparison of animals reasonable. Third, atropine is unlikely to have an effect on peripheral vascular blood flow dynamics beyond impacts on cardiac output due to a lack of parasympathetic tonus on the vessels. Although outside of the scope of this publication, it would be interesting to explore more selective muscarinic (M) receptor antagonists or nicotinic (N) receptor antagonists to more specifically block intestinal motility.

Of similar concern is whether alteration of cardiovascular function in the context of administration of chemotherapeutics which may elicit cardiotoxicity could impact peripheral vascular function and therefore outcome of data acquired using the proposed microbubble technique. However, in our study we did not observe animals with cardiovascular abnormalities, so we cannot rule out this potential. Future study of this aspect is certainly of interest but is beyond the scope of this publication.

The proposed 3D ultrasound technique also has limitations that need to be considered during experimental design. First, the 3D Motor used for the 3D reconstructions on the Vevo 2100 ultrasound imaging system has a maximal scan length of 35 mm (Figures 1 and 2c). In C57BL/6 mice, this enabled the reconstruction of the mid and distal colon in mice weighing approximately <30 g. Animals approximately >30 g resulted in reconstructions that were limited in the cranial direction but still encompassed the majority of the mid and distal colon. Second, the penis/vagina and pelvic bridge creates a distal shadow that obstructs the colon image as the 3D Motor passes over this region during image acquisition (Figure 6, Supplementary Video S1). In male mice (Figure 6d), this shadow is more pronounced and interfered with more frames than in female mice (Figure 6c). Tilting the mouse slightly to the left or right so that the angle of the transducer approaches from the side helps somewhat, but loss of frames in this region can be unavoidable. Therefore, when the user defines the ROI tissue structures of the colon wall and tumor, those frames that appear dark due to reproductive tract interference are simply avoided and left undefined. While this does admittedly exclude a small window of data, it is not a large number of frames (~5–10 frames in females and ~15–30 frames in males) when compared with the total of 344 frames collected (see Supplementary Video S1). Because the presence of these interfering structures is consistent, animals can be fairly compared. Finally, administration of US gel to the colon via the anus can result in gut perforation and death of the animal. However, in the course of our studies we caused the death of only one mouse by accidental colon perforation when injecting US gel into the colon (<1% mortality rate). The careful and slow introduction of the US gel with well-lubricated tubing is critical. While the 3D reconstruction technique can feasibly be performed as often as needed for the given experiment, it is our suggestion that acquisition be limited to once weekly. In the context of AOM/DSS-induced CRC, the tumors do not grow rapidly enough to warrant more than weekly ultrasound.[43] Additionally, animals with CRC tumors can exhibit poor overall health. Increasing the frequency of fasting and introduction of stress from handling and anesthesia can decrease mouse survival.

We provided a detailed method for performing 3D ultrasound in a murine model of colon cancer using the Vevo 2100 high-resolution ultrasound system. This study included preparation of the animal for imaging, 3D image acquisition, the use of VevoLAB software for 3D reconstruction analysis of colon walls and tumor volumes, and also the use of microbubbles for NLC imaging for the analysis of relative vascularity. Comparison of 3D ultrasound to traditional 2D photographs demonstrates the utility of the technique, adding a useful tool to the researcher's toolbox. Failure of the translation of colon cancer therapy from mouse to human can at least in part be attributed to the lack of ability to quantifiably track tumor progression in real-time in the mouse model. Our noninvasive, trans-abdominal ultrasound imaging method can be performed repeatedly without major complications while monitoring CRC with maximal accuracy. Endpoint-only evaluations of CRC may miss valuable information about treatment windows critical to finding clinically relevant treatment therapies. The 3D ultrasound can quantify the dynamics of tumor growth in mice, record their individual responses to treatment, and significantly reduce the number of mice needed per designed experiment.

MATERIALS AND METHODS

Imaging equipment

The Vevo 2100 High Resolution Micro-Ultrasound System with MS550S and MS250 transducers and VevoLAB software was used for this study (FUJIFILM VisualSonics, Toronto, ON, Canada). 3D Mode and Motor with associated 3D reconstruction software and NLC Mode with associated VevoCQ software was employed for data collection and extraction, respectively. 3D Mode and NLC Mode were combined to produce images to enable percent agent (PA) calculations. The higher resolution MS550S transducer was used for the 3D colon reconstructions acquiring data at 32–56 MHz with a maximal depth of 13 mm. The MS250 transducer which acquires data at a lower frequency of 13–24 MHz was used for acquisition of 2D and 3D NLC Mode Images. The transducer was controlled by the 3D Motor which maintained slow and incremental movement of the transducer to obtain ~300 frames with a step size of 0.1 mm and a maximal scan length of 35 mm. We did not find it necessary to activate respiratory gating for the method of 3D reconstruction performed with the MS550S transducer (Figure 2), as we found image quality to be sufficient and acquisition time was dramatically decreased without gating. Respiratory gating was however activated for the pre and postscans being performed for 3D NLC PA relative vascularity acquisitions with the MS250 transducer. Respiratory gating was suspended during microbubble infiltration for 2D NLC relative blood perfusion and blood volume analysis.

Animals and preparation

All experiments were conducted with institutional animal care and use committee approval. We used male and female C57/BL6 mice (Envigo, Denver, CO). A timeline is provided in Figure 4e. CRC was induced in the mice at 8 weeks of age. Animals were subsequently imaged 5 weeks after induction of CRC and this time-point defined as pretreatment. At pretreatment, a 3D Mode colon reconstruction was performed with the higher-resolution MS550S transducer. Five weeks after the beginning of treatment, animals again underwent 3D Mode colon reconstruction with the MS550S transducer and this time-point defined as post-treatment. Two weeks later at the terminal time-point, a 3D colon reconstruction was performed with the MS550S transducer, followed by evaluation of relative vascularity using 3D NLC PA and relative blood perfusion and volume using 2D NLC wash-in of microbubbles.

Animals were fasted for a minimum of 16 hours prior to imaging. For the pre-echo and post-echo time points, mice were lightly anesthetized with Isoflurane anesthesia, fixed with tape to the ultrasound platform, and the body temperature maintained. Anesthesia was lightly maintained and in a consistent fashion between animals so as to not inhibit cardiovascular function or confound values of relative colon vascularity, blood perfusion, and volume. The entire abdomen was removed of hair using depilatory cream with particular care taken to remove the hair around the anus and reproductive organs.

To inhibit peristalsis and improve imaging quality, a slow-release form of Atropine was administered (#A0132, Sigma-Aldrich, St. Louis, MO) 0.02 mg/ml 100–150 µl SC, ~5 minutes prior to the start of 3D reconstruction imaging. This dose takes effect after 5 minutes and lasts for ~15 minutes, providing sufficient time for the 3D Mode colon reconstructions at the pre and post-treatment time-points. However, an additional dose of another 100–150 µl SC was administered at the terminal time-point to extend blockage of peristalsis for the added 2D NLC and 3D NLC imaging.

To enable sufficient contrast to differentiate the colon from the surrounding abdominal tissues, US gel (Aquasonic, Fairfield, NJ) was introduced retrograde into the colon via the anus. A 3 ml syringe (BD Wordlwide, Franklin Lakes, NJ) was prepared by filling with standard US gel and slow centrifugation to remove air bubbles. The syringe was then fitted with a 20 G needle (BD Wordlwide) with a 1.5 inches length of polyethylene (PE) 60 tubing (BD Wordlwide) threaded over the needle to serve as a catheter to deliver the US gel to the colon. Immediately after the administration of atropine, the exterior of the PE60 tubing was lubricated with more US gel, and the tubing gently introduced into the anus of the mouse. Introduction of ~1–2 ml of US gel to the anus immediately following the injection of atropine was crucial as this enabled the US gel to help to expel any remaining feces from the colon, before the atropine took effect and while peristalsis was still active. Care was

taken to keep the tubing in-line with the natural directionality of the colon and to not penetrate the colon too deeply and cause wall puncture. Once atropine had taken effect, additional US gel was introduced to the colon as needed via the anus to optimize the image. However, we found that given the risk of intestinal puncture, to keep the number of gel introductions to a maximum of two to three. Application of US gel at the base of the tail to build-up gel in the area around the anus was critical to clear reconstructions of the anus and associated tumors.

Testing treatment paradigm

Figure 4e defines the treatment timeline. A combination AOM and DSS compounds (MP Biomedicals LLC, Irvine, CA) were used to model inducible CRC. Mice were administered a single injection of AOM (10 mg per/kg body weight) by IP injection followed by 1 week of rest. DSS (2% in the drinking water) was then administered in the drinking water for 1 week.[44] We were able to detect initial tumors 5 weeks after the single dose AOM injection and fully matured tumors 11 weeks after AOM injection in AOM/DSS treated C57Bl/6 mice.[6] The anticancer effect of an antitumorigenic compound (TX) under investigation in our group was tested for comparison of ultrasound accuracy. Five weeks following the AOM injection and prior to beginning vehicle or treatment (VEH or TX), a pretreatment ultrasound was collected. Treatment with VEH or TX was continued for 4 weeks and a post-treatment ultrasound taken. A terminal ultrasound and necropsy was performed 2 weeks after the post-treatment ultrasound.

Microbubble administration

Nontargeted microbubble administration was performed at the terminal end point only. Mice were anesthetized with Isoflurane anesthesia (Piramal, Bethlehem, PA) and orally intubated and ventilated to facilitate improved neck access. The left external jugular vein was surgically exposed and isolated. The stretched-end of a heparinized, 3 inch segment of PE20 tubing (BD Wordlwide) was introduced into the vein and sutured in place. 50 µl of heparinized saline (Hospira, San Jose, CA) was then injected to verify catheter patency. Animals were then extubated and transferred to the heated ultrasound platform and maintained by mask on Isoflurane at 1.5%. Note that a minimum concentration of anesthetic gas is essential to prevent perturbation of physiology. Additionally, keeping a consistent anesthetic level between animals is critical to reliable vascular data outcomes. To prepare for injection, 40 µl of undiluted SIMB3-4 microbubbles (Advanced Microbubble Laboratories LLC, Boulder, CO) were slowly drawn up in a syringe from the vented and gently mixed vial. Care was taken to prevent microbubble rupture due to pressure changes. At initiation of imaging requiring microbubble injection, the PE20 tubing was again flushed with a small amount of heparinized saline. Once the required imaging sequence was initiated, the microbubble bolus was injected via the jugular catheter and the appropriate images recorded. While we utilized hand-injection of bubbles, a syringe pump is strongly recommended for the bolus injection.

Comparison to standard colon photographs

At the terminal ultrasound, mice were not allowed to return to consciousness and the colons were removed, splayed opened longitudinally, washed with PBS, and secured with pins on the surface of silicone-coated dishes. Photographs were then taken using the Leica S6D stereomicroscope with EC3 digital camera (Leica Microsystems, Buffalo Grove, IL). Tumor surface areas were calculated using Leica LAS v4.8 software Analysis module.

3D mode image collections

As rationalized above, atropine was administered and the time noted. The atropine took effect after ~5 minutes and lasted for ~15 minutes. US gel was immediately delivered in a retrograde fashion to the colon via the anus to aid in elimination of any remaining feces prior to the atropine taking effect. With the transducer oriented in the sagittal plane, the length of the colon was identified and the image optimized on the screen. If fecal pellets were still present and interfering with the image quality, they were chased cranial around the flexure of the colon with more US gel after the atropine had taken effect. Adjustment of the MS550S transducer depth, medial/lateral, and cranial/caudal orientation was optimized to ensure that the entire length of the mid and distal colon was within the frame of the screen to ensure inclusion in the 3D Motor acquisition of the necessary 344 frames. Special care was also taken to locate and remove any air bubbles in the US gel on the exterior of the animal which may interfere with image clarity. Adequate intracolon US gel was present if the colon lumen appeared distended, black, and with the colon walls clearly identifiable. US gel administration to the anus was repeated if needed, but limited to two or three attempts to reduce risk of colon perforation. Once the image was optimized and intestinal peristalsis halted, the transducer was turned from sagittal to transverse. We did not activate respiratory gating for 3D Mode colon reconstruction with the MS550S transducer. However, respiratory gating is required for 3D NLC PA microbubble imaging. A 3D Motor scan was then collected with a scan distance of 34.950 mm, step size of 0.102 mm, and 344 total frames. As the image slices appeared on the screen, it was confirmed that the scan began far enough caudal that the entire anus was included in the scan and ended far enough anterior that the colon *flexure* was identified. The appearance of the *flexure* is very clear as the colon begins to turn laterally to the animal's right side with each successive image frame as the 3D motor travels in the cranial direction. If this was not confirmed, reoptimization was performed and the scan sequence repeated. The entire scan sequence was then captured using Cine Store and appropriately labeled.

NLC mode microbubble imaging

An additional dose of 100–150 µl SC of atropine was administered prior to NLC Mode imaging, as peristalsis was typically returned by the time the 3D Mode colon reconstruction had been completed. The MS250 transducer was then activated on the Vevo 2100 system. The animal was again prepared for 3D imaging as outlined above. Additional intracolon US gel was administered if needed to make sure the colon was distended and the colon walls were clearly visible. Note that the resolution of this probe is not as high as the MS550S probe but that the lower frequency of the MS250 probe is necessary for NLC image acquisition. A transverse 3D Mode prescan of the colon with NLC Mode and respiratory gating active was next obtained, appropriately named, and then saved. The transducer was then carefully turned to the sagittal orientation without changing the animal position or performing any more US gel administrations. The respiratory gating was then disabled and the system engaged using Scan/Freeze just prior to administration of the microbubbles. 40 µl of SIMB3-4 microbubbles were then administered through the jugular catheter (Bubble injection = Time 0 minutes). The wash-in of the bubbles, encompassing typically 300 frames and 17–20 seconds is then saved and labeled (2D NLC captured = Time 30 seconds). The transducer was then returned to the transverse orientation, again carefully to prevent movement of the animal, and the respiratory gating reactivated. After the bubbles have been allowed to circulate for ~2 minutes to ensure complete distribution, another 3D NLC postscan was collected and saved (3D postscan completed Time = 4 minutes). As the timeline indicates, all images were collected within ~ 4 minutes of administration of microbubbles, making acquisition of images consistent between animals and uninfluenced by variation in microbubble degradation. In our study, the microbubbles were only administered at the endpoint ultrasound, so tissues were collected and the animal was never allowed to return to consciousness. However, if microbubble administration is performed by an individual skilled at tail-vein injection, the animal may be returned to consciousness with no negative effects from the microbubble injection and imaging. Of important note, tail-vein delivered microbubble injections may be performed as often as necessary for the experimental protocol, without ill effects on animal health.

Image analysis

3D software colon reconstruction. Images acquired with the MS550S transducer were loaded into VevoLAB 3D software. An optional but helpful, Wacom Cintiq 22HD tablet with pen (Wacom Technology, Vancouver, WA) was utilized to assist with colon reconstructions. After loading the acquired images, the software automatically assimilated the images into a 3D reconstruction. However, manual definition of colon walls and tumors is required for volumetric quantification. In *Cube View* the first image of the stack where the anus was clearly visible was then aligned in the plane of the screen facing the user. The *volume* and *parallel* functions were then used to define the ROI of the outer wall of the colon frame-by-frame, repeating until the first frame of the colon *flexure* became visible indicating the approach of the proximal colon. The *anus* to *flexure* landmarks enabled consistency in defining the colon length between animals. We found it unnecessary to define the object of interest in every frame, with every 5–10 frames proving sufficient. The inner wall definitions were then repeated using the same process. Finally, tumors were identified and defined, individually. The software then output a separate volume value for each individual defined object. Therefore, individual tumors as small as 0.5 mm^3 were quantified, and total tumor burden

was quantified by the summing of all the tumors. Additionally, subtraction of outer and inner wall volumes enabled quantification of total colon volume indicative of changes in colon thickness due to potential inflammation. Although not presented here, the software also encompasses the ability to extract other data such as colon length from the reconstruction.

2D NLC relative blood perfusion and volume analysis. Sagittal images acquired using the MS250 transducer as the microbubbles infiltrated the colon with NLC activated were loaded into the VevoCQ software. The collected video typically encompassed 270 frames and 17 seconds. The video included several seconds prior to injection of the bubbles through several seconds after the bubbles reached circulation stasis (Supplementary Video S3). A motion corrected clip was obtained and no frames were excluded from analysis. A ROI was defined and the entire sagittal colon length segment was included in analysis. The *Origin of Arrival* was defined as the location at which the slope began to launch upwards. The software calculated the slope (wash-in rate and relative blood perfusion) and plateau (relative blood volume) among additional parameters not presented here.

3D NLC PA analysis. The transverse 3D Mode NLC prescan image set acquired with the MS250 transducer was loaded into the 3D reconstruction software. The software automatically assimilated the images into a 3D image as explained previously. In *Cube View* the first image of the stack was then aligned in the plane of the screen facing the user. The *volume* and *parallel* functions were then used to encircle the region extending outside of the outer wall of the colon, thereby defining the ROI frame-by-frame to include the vascular bed encompassing the colon walls. However as before, we found it unnecessary to define the object of interest in every frame and every 5–10 frames proved sufficient. Once the ROI has been defined in a sufficient number of frames to enable definition of the entire length of collected colon data, the collected ROI data was *copied*. Then the postscan was loaded into the software and this *copied* data was *pasted* onto the postscan. The PA values from the pre and postscans were then subtracted to yield the final 3D NLC PA value of the colon.

An important point during this procedure is that some movement of the colon may have occurred between the pre and postscans, even with repeated administration of atropine. However, this movement can be accounted for within the software by redefining the individual location of each colon wall ROI in each frame once the *copy-and-paste* has been completed. This can be accomplished without changing the shape or size of each ROI but by simply dragging it to the location where the colon has migrated.

CONFLICT OF INTEREST

The authors declare no conflicts of interest.

ACKNOWLEDGMENTS

We thank the Physiology Core Facility at the University of South Dakota, Department of Basic Biomedical Sciences for the use of the ultrasound equipment and supplies. This work was supported by a startup package (Division of Basic Biomedical Sciences, University of South Dakota) and by National Institute of General Medical Sciences of the National Institutes of Health (NIH) award 5P20GM103548 (Miskimins) to KSR.

REFERENCES

1. Siegel, R, Desantis, C and Jemal, A (2014). Colorectal cancer statistics, 2014. *CA Cancer J Clin* **64**: 104–117.
2. El Zoghbi, M and Cummings, LC (2016). New era of colorectal cancer screening. *World J Gastrointest Endosc* **8**: 252–258.
3. Arnold, M *et al.* (2016). Global patterns and trends in colorectal cancer incidence and mortality. *Gut* doi:10.1136/gutjnl-2015-310912.
4. Kerr, D (2003). Clinical development of gene therapy for colorectal cancer. *Nat Rev Cancer* **3**: 615–622.
5. Richmond, A and Su, Y (2008). Mouse xenograft models vs GEM models for human cancer therapeutics. *Dis Model Mech* **1**: 78–82.
6. De Robertis, M, Massi, E, Poeta, ML, Carotti, S, Morini, S, Cecchetelli, L *et al.* (2011). The AOM/DSS murine model for the study of colon carcinogenesis: from pathways to diagnosis and therapy studies. *J Carcinog* **10**: 9.
7. Mittal, VK, Bhullar, JS and Jayant, K (2015). Animal models of human colorectal cancer: current status, uses and limitations. *World J Gastroenterol* **21**: 11854–11861.
8. Neufert, C, Becker, C and Neurath, MF (2007). An inducible mouse model of colon carcinogenesis for the analysis of sporadic and inflammation-driven tumor progression. *Nat Protoc* **2**: 1998–2004.
9. McIntyre, RE, Buczacki, SJ, Arends, MJ and Adams, DJ (2015). Mouse models of colorectal cancer as preclinical models. *Bioessays* **37**: 909–920.
10. Xue, Y, Johnson, R, Desmet, M, Snyder, PW and Fleet, JC (2010). Generation of a transgenic mouse for colorectal cancer research with intestinal cre expression limited to the large intestine. *Mol Cancer Res* **8**: 1095–1104.
11. Karim, BO and Huso, DL (2013). Mouse models for colorectal cancer. *Am J Cancer Res* **3**: 240–250.
12. Rosenberg, DW, Giardina, C and Tanaka, T (2009). Mouse models for the study of colon carcinogenesis. *Carcinogenesis* **30**: 183–196.
13. Jackstadt, R and Sansom, OJ (2016). Mouse models of intestinal cancer. *J Pathol* **238**: 141–151.
14. Adachi, T, Hinoi, T, Sasaki, Y, Niitsu, H, Saito, Y, Miguchi, M *et al.* (2014). Colonoscopy as a tool for evaluating colorectal tumor development in a mouse model. *Int J Colorectal Dis* **29**: 217–223.
15. Becker, C, Fantini, MC and Neurath, MF (2006). High resolution colonoscopy in live mice. *Nat Protoc* **1**: 2900–2904.
16. Hensley, HH, Merkel, CE, Chang, WC, Devarajan, K, Cooper, HS and Clapper, ML (2009). Endoscopic imaging and size estimation of colorectal adenomas in the multiple intestinal neoplasia mouse. *Gastrointest Endosc* **69**(3 Pt 2): 742–749.
17. Alencar, H, King, R, Funovics, M, Stout, C, Weissleder, R and Mahmood, U (2005). A novel mouse model for segmental orthotopic colon cancer. *Int J Cancer* **117**: 335–339.
18. Young, MR, Ileva, LV, Bernardo, M, Riffle, LA, Jones, YL, Kim, YS *et al.* (2009). Monitoring of tumor promotion and progression in a mouse model of inflammation-induced colon cancer with magnetic resonance colonography. *Neoplasia* **11**: 237–46, 1p following 246.
19. Choquet, P, Calon, A, Breton, E, Beck, F, Domon-Dell, C, Freund, JN *et al.* (2007). Multiple-contrast X-ray micro-CT visualization of colon malformations and tumours in situ in living mice. *C R Biol* **330**: 821–827.
20. Vakoc, BJ, Fukumura, D, Jain, RK and Bouma, BE (2012). Cancer imaging by optical coherence tomography: preclinical progress and clinical potential. *Nat Rev Cancer* **12**: 363–368.
21. Soletti, RC, Alves, KZ, de Britto, MA, de Matos, DG, Soldan, M, Borges, HL *et al.* (2013). Simultaneous follow-up of mouse colon lesions by colonoscopy and endoluminal ultrasound biomicroscopy. *World J Gastroenterol* **19**: 8056–8064.
22. Barbieri, A, Barretta, ML, Rea, D, Picone, C, Fabozzi, O, Palma, G *et al.* (2013). Intraluminal gel ultrasound and eco-color doppler: new tools for the study of colorectal cancer in mice. *In Vivo* **27**: 443–450.
23. Crncec, I, Pathria, P, Svinka, J and Eferl, R (2015). Induction of colorectal cancer in mice and histomorphometric evaluation of tumors. *Methods Mol Biol* **1267**: 145–164.
24. Ma, X, Yan, F, Deng, Q, Li, F, Lu, Z, Liu, M *et al.* (2015). Modulation of tumorigenesis by the proinflammatory microRNA miR-301a in mouse models of lung cancer and colorectal cancer. *Cell Discov* **1**: 15005.
25. Nguyen, TL, Vieira-Silva, S, Liston, A and Raes, J (2015). How informative is the mouse for human gut microbiota research? *Dis Model Mech* **8**: 1–16.
26. Treuting, PM, Dintzis, SM, Frevert, CW, Liggitt, HD and Montine, KS. *Comparative Anatomy and Histology: A Mouse and Human Atlas*, Elsevier/Academic Press, Amsterdam: Boston; 2012.
27. Fernandes, T, Oliveira, MI, Castro, R, Araújo, B, Viamonte, B and Cunha, R (2014). Bowel wall thickening at CT: simplifying the diagnosis. *Insights Imaging* **5**: 195–208.
28. Niermann, KJ, Fleischer, AC, Huamani, J, Yankeelov, TE, Kim, DW, Wilson, WD *et al.* (2007). Measuring tumor perfusion in control and treated murine tumors: correlation of microbubble contrast-enhanced sonography to dynamic contrast-enhanced magnetic resonance imaging and fluorodeoxyglucose positron emission tomography. *J Ultrasound Med* **26**: 749–756.
29. Gately, S, Twardowski, P, Stack, MS, Patrick, M, Boggio, L, Cundiff, DL *et al.* (1996). Human prostate carcinoma cells express enzymatic activity that converts human plasminogen to the angiogenesis inhibitor, angiostatin. *Cancer Res* **56**: 4887–4890.
30. Wali, RK, Roy, HK, Kim, YL, Liu, Y, Koetsier, JL, Kunte, DP *et al.* (2005). Increased microvascular blood content is an early event in colon carcinogenesis. *Gut* **54**: 654–660.
31. Carmeliet, P and Jain, RK (2011). Principles and mechanisms of vessel normalization for cancer and other angiogenic diseases. *Nat Rev Drug Discov* **10**: 417–427.
32. Foster, FS, Hossack, J and Adamson, SL (2011). Micro-ultrasound for preclinical imaging. *Interface Focus* **1**: 576–601.
33. Graham, KC, Wirtzfeld, LA, MacKenzie, LT, Postenka, CO, Groom, AC, MacDonald, IC *et al.* (2005). Three-dimensional high-frequency ultrasound imaging for longitudinal evaluation of liver metastases in preclinical models. *Cancer Res* **65**: 5231–5237.
34. Deshpande, N, Lutz, AM, Ren, Y, Foygel, K, Tian, L, Schneider, M *et al.* (2012). Quantification and monitoring of inflammation in murine inflammatory bowel disease with targeted contrast-enhanced US. *Radiol* **262**: 172–180.
35. Machtaler, S, Knieling, F, Luong, R, Tian, L and Willmann, JK (2015). Assessment of inflammation in an acute on chronic model of inflammatory bowel disease with ultrasound molecular imaging. *Theranostics* **5**: 1175–1186.

36. Sirsi, S, Feshitan, J, Kwan, J, Homma, S and Borden, M (2010). Effect of microbubble size on fundamental mode high frequency ultrasound imaging in mice. *Ultrasound Med Biol* **36**: 935–948.
37. Streeter, JE, Gessner, R, Miles, I and Dayton, PA (2010). Improving sensitivity in ultrasound molecular imaging by tailoring contrast agent size distribution: *in vivo* studies. *Mol Imaging* **9**: 87–95.
38. Hyvelin, JM, Tardy, I, Arbogast, C, Costa, M, Emmel, P, Helbert, A *et al.* (2013). Use of ultrasound contrast agent microbubbles in preclinical research: recommendations for small animal imaging. *Invest Radiol* **48**: 570–583.
39. Willmann, JK, Paulmurugan, R, Chen, K, Gheysens, O, Rodriguez-Porcel, M, Lutz, AM *et al.* (2008). US imaging of tumor angiogenesis with microbubbles targeted to vascular endothelial growth factor receptor type 2 in mice. *Radiol* **246**: 508–518.
40. Tiwari, AK, Crawford, SE, Radosevich, A, Wali, RK, Stypula, Y, Kunte, DP *et al.* (2011). Neo-angiogenesis and the premalignant microcirculatory augmentation of early colon carcinogenesis. *Cancer Lett* **306**: 205–213.
41. Rea, D, Coppola, C, Barbieri, A, Monti, MG, Misso, G, Palma, G *et al.* (2016). Strain analysis in the assessment of a mouse model of cardiotoxicity due to chemotherapy: sample for preclinical research. *In Vivo* **30**: 279–290.
42. Milano, G, Raucci, A, Scopece, A, Daniele, R, Guerrini, U, Sironi, L *et al.* (2014). Doxorubicin and trastuzumab regimen induces biventricular failure in mice. *J Am Soc Echocardiogr* **27**: 568–579.
43. Thaker, AI, Shaker, A, Rao, MS and Ciorba, MA (2012). Modeling colitis-associated cancer with azoxymethane (AOM) and dextran sulfate sodium (DSS). *J Vis Exp* (67): e4100. doi:10.3791/4100.
44. Tanaka, T, Kohno, H, Suzuki, R, Yamada, Y, Sugie, S and Mori, H (2003). A novel inflammation-related mouse colon carcinogenesis model induced by azoxymethane and dextran sodium sulfate. *Cancer Sci* **94**: 965–973.

Supplementary Information accompanies this paper on the *Molecular Therapy—Methods & Clinical Development* website (http://www.nature.com/mtm)